Analyst

PAPER

Cite this: *Analyst*, 2016, **141**, 5879

# A mechanical pencil lead-supported carbon nanotube/Au nanodendrite structure as an electrochemical sensor for As(III) detection†

Pham Khac Duy,[a] Jong-Ryeul Sohn[b] and Hoeil Chung*[a]

A mechanical pencil lead (MPL), an easily obtainable carbon-based material with a consistent size, was used as a frame to construct an MPL-supported carbon nanotube/Au nanodendrite (MPL-CNT/AuND) sensor through simple electrodeposition of Au onto the MPL in the presence of CNTs. A nanodendrite structure was adopted to ensure large numbers of active electrochemical sites because of its hierarchical structure with well-aligned terraces; the CNTs were used to firmly adhere the fabricated Au nanodendrites to the MPL surface to ensure ruggedness. The MPL-CNT/AuND structure was used to measure $As^{3+}$ samples in a concentration range from 0.5 to 80 ppb using anodic stripping voltammetry (ASV). The variation in peak intensities was linear ($R^2$: 0.997), and the limit of detection (LOD) was 0.4 ppb. The average relative standard deviation (RSD) of the peak intensities from the voltammograms of each sample collected using three separately prepared MPL-CNT/AuNDs was 8.7%, thereby demonstrating good sensor-to-sensor reproducibility. Furthermore, when three $As^{3+}$ samples prepared in tap water were measured, the accuracy was maintained without noticeable degradation and the response was steady up to 50-cycle measurements.

Received 6th April 2016,
Accepted 22nd June 2016

DOI: 10.1039/c6an00803h

www.rsc.org/analyst

## Introduction

Carbon-based materials such as carbon paste and glassy carbon, some of the most common materials used to prepare electrodes, have been widely utilized in various electrochemical analyses.[1–4] In addition, the demand for inexpensive, easy-to-fabricate, and field-usable electrochemical sensors, especially for on-site measurements, has been gradually increasing. In this context, pencil lead, another carbon-based material, has gained attention because it is inexpensive and readily available, with uniform quality.[5–12] Therefore, diverse electrochemical measurements utilizing pencil leads have been reported, including the use of Ag- and AgCl-doped pencil lead as a reference electrode in a paper-based device[13] and the use of a pencil-lead working electrode for the measurements of analytes (*e.g.*, antioxidants, dopamine, and uric acid) in garlic, fruit, and vegetable extracts.[14] To further enhance the use of pencil leads for analysis, researchers have fabricated additional structures on them, such as a multiwall carbon nanotube/polyaniline structure as a bio-cathode for an enzymatic bio-fuel cell,[15] electro-polymerized Eriochrome Black T for the simultaneous examination of the oxidation behaviors of dopamine and uric acid,[16] and polypyrrole as a nitrate-sensitive ion-selective electrode.[17]

Researchers have also fabricated metallic nanostructures on pencil leads to enhance their performance in electrochemical sensing by taking advantage of nanostructures' properties such as large surface areas and excellent conductivities. In particular, Au nanoparticles (AuNPs) have been a frequently adopted choice for this purpose. AuNP-incorporated pencil leads have been used, for example, to determine the hydrogen peroxide concentrations in hair dyes and disinfectants[18] and to monitor glucose in the hydrolysis of waste tree branch over extended periods.[19] In addition, pencil-graphite-supported Au nanorod electrodes have been developed and used to detect anti-HIV drugs[20] and DNA.[21]

With respect to metallic nanostructures to be fabricated on a pencil lead, a material that provides a larger surface area is advantageous and its fabrication should be simple, without involving complex synthesis steps. Given these requirements, the nanodendrites of a hierarchical structure with a high population of active electrochemical sites would be a potential candidate.[22,23] Therefore, we here demonstrate a mechanical pencil lead (MPL)-supported carbon nanotube/Au nano-

[a]*Department of Chemistry and Institute for Materials Design, College of Natural Sciences, Hanyang University, Seoul, 04763, Korea. E-mail: hoeil@hanyang.ac.kr; Tel: +82 2 2220 0937*

[b]*BK21PLUS Program in Embodiment: Health-Society Interaction, Department of Public Health Sciences, Graduate School, Korea University, Seoul 02841, Korea*

†Electronic supplementary information (ESI) available. See DOI: 10.1039/c6an00803h

dendrite structure (referred to as MPL-CNT/AuND) for the first time. For the fabrication, Au nanodendrites were constructed by simple electrodeposition onto an MPL in the presence of CNTs. The co-use of CNTs was to firmly adhere the formed Au nanodendrites to the MPL surface to make a physically rugged sensor. The structure of the MPL-CNT/AuND was characterized by scanning electron microscopy (SEM), and its electrochemical performance was evaluated in parallel with that of MPL-AuND, a structure fabricated without the use of CNTs. The fabricated MPL-CNT/AuND sensor was subsequently used to measure $As^{3+}$ samples in a concentration range from 0.5 to 80 ppb using anodic stripping voltammetry (ASV), and the sensor-to-sensor reproducibility was assessed through the analysis of the responses of three separately prepared sensors in each measurement. Furthermore, $As^{3+}$ samples prepared in tap water were also measured and the resulting accuracy was evaluated.

# Experimental

### Preparation of MPL-CNT/AuND sensor

Commercially available MPLs were purchased at a local stationery store. The dimensions of the MPLs were highly consistent, with a diameter and length of 0.5 and 60.0 mm, respectively. The MPLs were cut into lengths of 20 mm for sensor fabrication. Initially, a solution composed of 20 mM $HAuCl_4$, 0.5 M $H_2SO_4$, 1.0 mM KI, and 2.5 M $NH_4Cl$ was prepared, and then 0.3 mg CNTs (single wall; AP-grade; diameter: 1–1.2 nm; length: 2–20 μm) was added to this solution. The CNTs were purchased from Iljin Nanotech, Korea. The resulting solution was sonicated for 15 min to ensure thorough dispersion of the added CNTs. For the electrodeposition of Au, a 10 mm portion of MPL was immersed into the CNT-dispersed $Au^{3+}$ solution and a potential of −1.0 V was applied to the MPL for 180 s using a potentiostat. The constructed MPL-CNT/AuND structures were examined by SEM (Hitachi S-4800 SEM, Japan) and TEM; their relevant elemental mapping images were recorded during the TEM experiments (JEM-2100F TEM, JEOL, Japan).

### Arsenic sample preparation and electrochemical measurements using MPL-CNT/AuND sensors

As(III) solutions were prepared by using a standard solution purchased from Kanto Chemical Co., Inc. (Tokyo, Japan). This stock solution was tightly sealed and stored in the dark for further use. Different $As^{3+}$ samples in a desired concentration range (0.5 to 80 ppb) were prepared by properly diluting the 1000 ppm stock solution immediately before measurement. The total volume of each sample was 40 mL after the addition of the supporting electrolytes (50 μL 17.5% HCl and 70 μL 98% $H_2SO_4$).

ASV was used to measure the prepared $As^{3+}$ samples. Sample enrichment was previously performed by applying −0.4 V (*vs.* Ag/AgCl) to the MPL-CNT/AuND sensor with stirring over a period of 180 s, and voltammograms were acquired in the scan range from −0.3 to 0.6 V. All electrochemical measurements were carried out at room temperature using Ag/AgCl and Pt wire as reference and counter electrodes, respectively.

# Results and discussion

### Examination of MPL-CNT/AuND structure

The fabrication of Au nanodendrites on bare MPLs was initially attempted. For this purpose, a potential of −1.0 V was applied to the MPL in the $Au^{3+}$ solution without CNTs to initiate electrodeposition of Au; an SEM image of the fabricated structure (referred to as MPL-AuND) is shown in Fig. 1(a). The structure fabricated on the left of the MPL contained pores with sizes ranging from 20 to 30 μm. The pores resulted from hydrogen bubbles simultaneously generated at the surface by the reduction of $H^+$ during Au deposition.[22] When we examined the structure on the few-micron scale (Fig. 1(b)), we confirmed the construction of networked Au nanodendrites. However, the Au nanodendrites covered only the left part of the MPL surface; detached Au nanodendrite blocks are observed in the right side of the image (Fig. 1(a)). Even after eight repeated trials, the brown-color nanodendrites easily detached from the surface because of insufficient

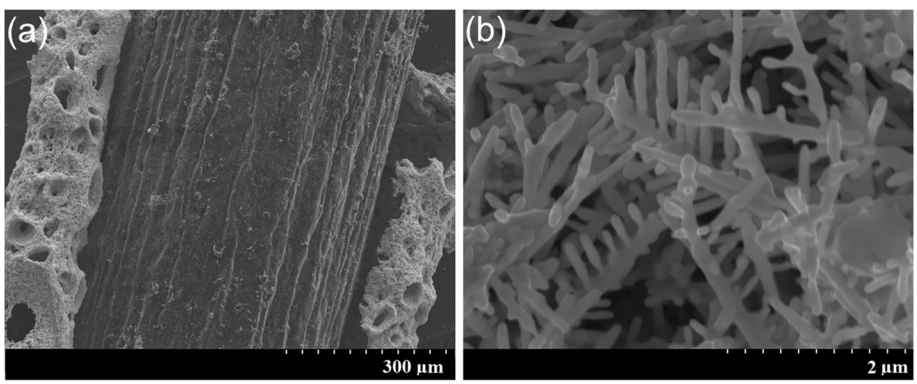


Fig. 1 SEM images of the MPL-AuND structure with two different fields of view.

adhesive power between the MPL and the Au nanodendrites. MPLs are known to consist mainly of graphite, with other components such as clay and wax added to fulfil the demanding functions of a pencil lead; the composition of MPLs varies depending on the types of pencil lead. Because a B-type MPL was used in this study, the mass percentages of graphite, clay, and wax were approximately 71%, 23%, and 5%, respectively.[24] The presence of clay and wax on the surface (totalling ~28%) is potentially disadvantageous in the surface adhesion of the metallic Au nanodendrite structure.

To increase the surface adhesive power, CNTs were used as a linker because they adhere better than Au nanodendrites to the MPL surface. In addition, CNTs are highly conductive materials with good chemical stability. We therefore performed the same electrodeposition but in the presence of CNTs. During the electrodeposition, the black solution containing both $Au^{3+}$ and dispersed CNTs gradually became clear, indicating the adsorption of CNTs onto the MPL *via* π–π interactions. Fig. 2(a) and (b) show photographs of a bare MPL (diameter: 0.5 mm) and an MPL-supported CNT/Au nanodendrite (MPL-CNT/AuND) structure, respectively. The formed Au nanodendrites exhibit a brown color and cover the MPL; no empty bare surface is observed. Fig. 2(c)–(f) show SEM images of the MPL-CNT/AuND structure with four different fields of view. The pores formed by hydrogen bubbles, which allow analytes to easily access the interior of the structure, thereby providing a fast electrochemical response, are also evident in the image with the largest field of view (Fig. 2(c)). The image of a single pore (Fig. 2(d)) reveals that the frame is a three-dimensional (3D) structure composed of networked nanodendrites. In the further magnified views (Fig. 2(e) and (f)), the nanodendrites with well-aligned terraces are clearly observed. The electrodeposition conducted over a period of 180 s produced the most characteristic nanodendrite shape, as shown in the images; by contrast, samples prepared using shorter or longer electrodeposition times resulted in immature or edge-blunt structures, respectively. The widths of the nanodendrites ranged from 700 to 800 nm, and their height reached approximately 3 μm. The diameters of both the trunks and the side branches were less than ~200 nm. Overall, the deposition of Au in the presence of CNTs resulted in stronger adherence of the Au nanodendrite structures to the MPL; in addition, the nanodendrite structure with a large active surface area should be beneficial for sensitive electrochemical measurements.

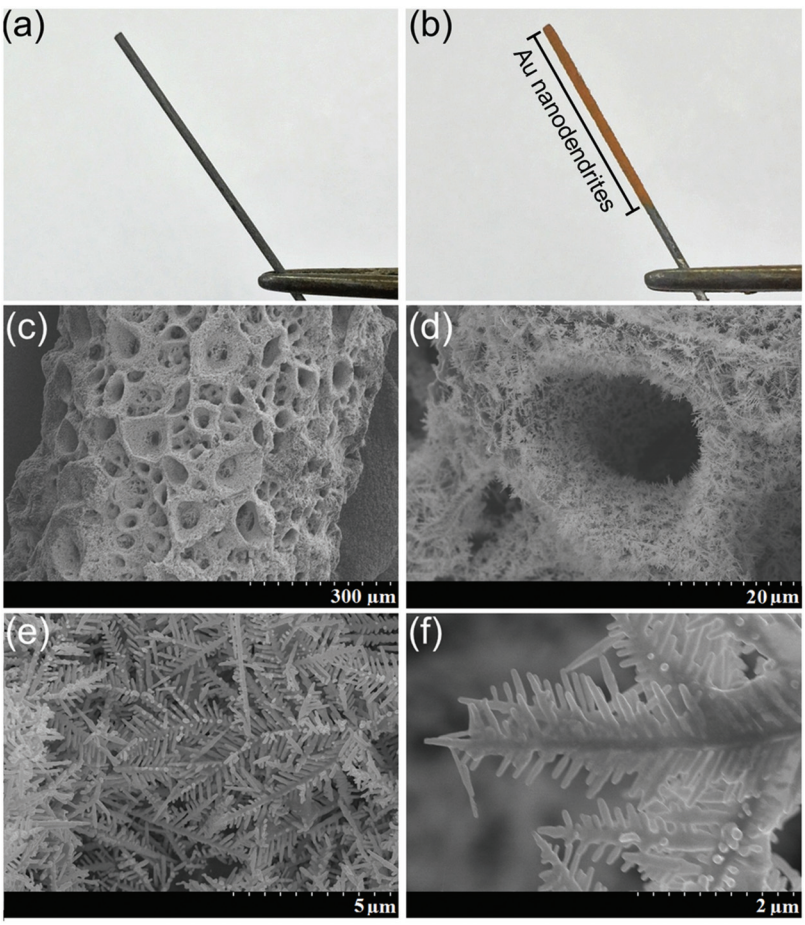


**Fig. 2** Photographs of a bare MPL (a) and MPL-CNT/AuND (b). SEM images of the MPL-CNT/AuND with four different fields of view are also presented (c)–(f).

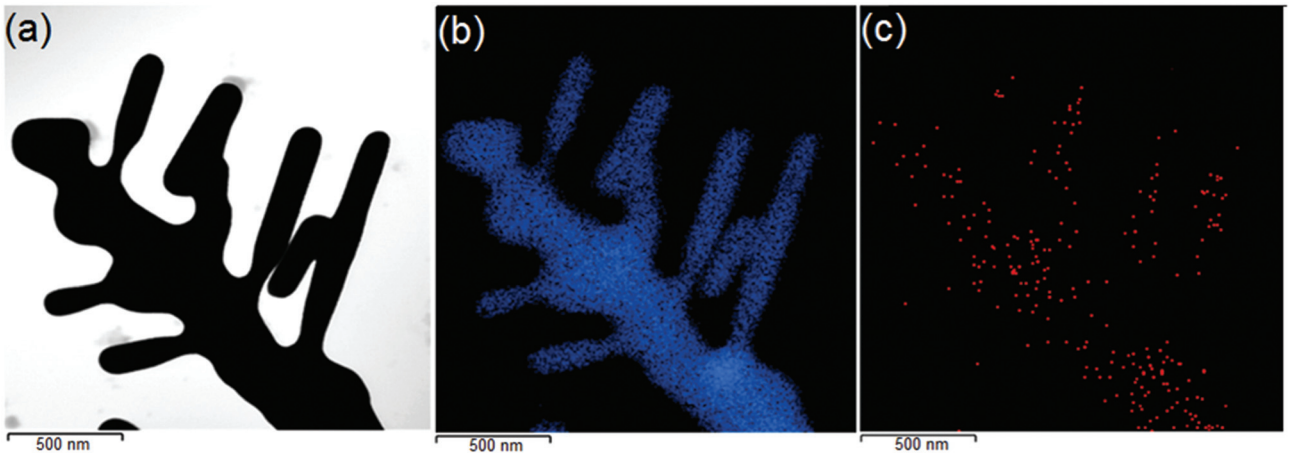


Fig. 3 TEM image of the top part of a single Au nanodendrite (a) and the corresponding elemental mapping images of Au (b) and carbon (c).

For further characterization, the top part of a single nanodendrite was observed by TEM and the corresponding elemental mapping images of Au and C were collected, as shown in Fig. 3. In the TEM image shown in Fig. 3(a), the terraces on the main dendritic column are apparent. In the Au (b) and C (c) mapping images, the relevant color is uniformly distributed over the structure in each case, thereby confirming the homogeneous distribution of both components over the nanodendrite. Although the CNT content was low, the partial incorporation of CNTs into the Au nanodendrite resulted in a more rugged MPL-CNT/AuND structure.

### Evaluation of electrochemical performance of MPL-CNT/AuND

To examine the electrochemical performance of the MPL-CNT/AuND sensor, its cyclic voltammogram (CV) in a 0.5 M $H_2SO_4$ solution was collected using a scan rate of 0.1 V $s^{-1}$. For comparison, the CV of MPL-AuND was collected under the same conditions. The best MPL-AuND among eight synthesized MPL-AuNDs was chosen for the measurement. As shown in Fig. 4(a), both CVs exhibit typical features of polycrystalline Au in $H_2SO_4$, including a cathodic peak at approximately 0.8 V; their intensities, however, greatly differ, as expected. The MPL-CNT/AuND provided approximately six-fold greater intensity compared to that of the MPL-AuND. The presence of uncovered surface with Au nanodendrites was responsible for the diminished intensity in the measurement using the MPL-AuND. A reduction peak at approximately 0.4 V, which corresponds to the CNT, was observed in the CV of MPL-CNT/AuND, thereby indicating the incorporation of CNTs into the structure, consistent with the finding in the elemental mapping images.

Next, a diffusional electrode area ($A_{diff}$) corresponding to the effective surface area available for a given electrochemical reaction, as estimated on the basis of the diffusion of an analyte, was calculated using the Randles–Sevcik equation:[25]

$$i_p = 2.69 \times 10^5 n^{3/2} D^{1/2} A_{diff} C \nu^{1/2}$$

Here, $i_p$ is the peak current corresponding to the reduction of the redox species, $n$ is the number of electrons transferred in the redox event, $D$ is the diffusion coefficient of the analyte, $C$ is the molar concentration of the analyte, and $\nu$ is the scan rate in V $s^{-1}$. For the calculation, CVs of the redox couple of

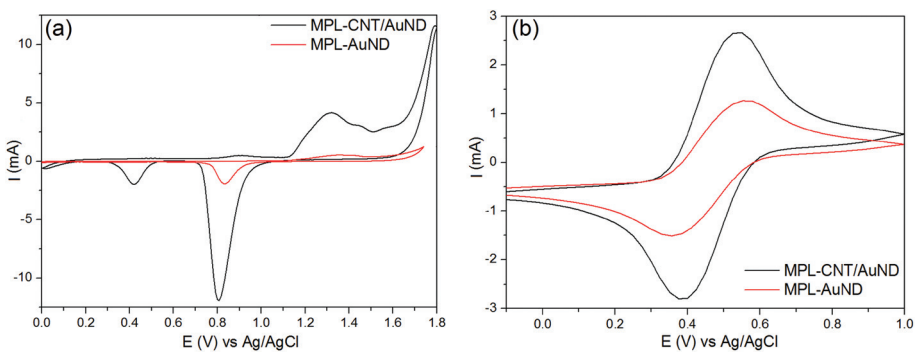


Fig. 4 CVs collected using MPL-AuND (red) and MPL-CNT/AuND (black) sensors in a 0.5 M $H_2SO_4$ solution at a scan rate of 0.1 V $s^{-1}$ (a); CVs of the $[Fe(CN)_6]^{3-}/[Fe(CN)_6]^{4-}$ redox couple (concentration: $5 \times 10^{-3}$ M), as acquired using the same electrodes (b).

 

$[Fe(CN)_6]^{3-}/[Fe(CN)_6]^{4-}$ were recorded using both MPL-AuND and MPL-CNT/AuND electrodes, as shown in Fig. 4(b). Three $K_3[Fe(CN)_6]$ samples of $1.0 \times 10^{-3}$, $2.5 \times 10^{-3}$ and $5 \times 10^{-3}$ M were separately measured for the calculation with a $D$ value of $7.5 \times 10^{-6}$ $cm^2$ $s^{-1}$. In both cases, reversible voltammograms were obtained and the peak current was apparently higher in the case of MPL-CNT/AuND. The average $A_{diff}$ for MPL-CNT/AuND was 2.36 $cm^2$. The current density calculated from the CV of the $[Fe(CN)_6]^{3-}/[Fe(CN)_6]^{4-}$ couple was 0.179 mA $mm^{-2}$, greater than that (0.094 mA $mm^{-2}$) of the Pt-supported Au nanodendrite, previously reported by our group.[22] The deposition of a thicker layer of Au nanodendrites and the larger pore size, which enables greater contact between the analyte and the electrode surface, were responsible for the observed increased current density. The ranges of pore sizes in the MPL-CNT/AuND and Pt-supported Au nanodendrite were 20–30 and 5–10 μm, respectively.

### Detection of As(III) using the MPL-CNT/AuND sensor

We used the MPL-CNT/AuND sensor to detect $As^{3+}$ ions in a concentration range from 0.5 to 80 ppb (a total of 10 samples). In addition, to evaluate the sensor-to-sensor reproducibility, we used three separately prepared MPL-CNT/AuND sensors to measure each sample. Fig. 5(a) shows the stripping voltammograms of the samples acquired using MPL-CNT/AuND. The intensities of the peaks at approximately 0.05 V clearly increased with increasing $As^{3+}$ concentration. Fig. 5(b) presents a plot of the $As^{3+}$ concentration *vs.* the peak intensity; this plot confirms that the intensity variation was linear ($R^2$: 0.997) in the tested concentration range and the calculated limit of detection (LOD) was 0.4 ppb. The inset shows the relative standard deviations (RSDs) of the peak intensities in the measurements of each sample using the three independent MPL-CNT/AuND sensors. As expected, the RSDs were greater in the cases of measuring samples with low analyte concentrations, such as 17.6% for the 0.5 ppb sample; however, the average RSD was 8.7%, indicative of good inter-sensor reproducibility. Further, the dynamic range of the sensor was evaluated by examining responses of $As^{3+}$ samples greater than 80 ppb and up to 800 ppb. The intensity variation was linear up to 800 ppb with $R^2$ of 0.994 (refer to ESI†), thereby the found dynamic range was 0.5–800 ppb.

Furthermore, the same CR-CNT/AuND sensors were used to measure three $As^{3+}$ samples (20, 40, and 60 ppb) prepared in real tap water and their concentrations were predicted (Table 1) using the calibration curve. Before the measurement, a tap water sample was filtered through a glass fiber filter to eliminate potential surrounding interferences such as suspend particulates and/or organic chemicals. Again, three CR-CNT/AuND sensors were separately used to measure each sample. As shown, the $As^{3+}$ concentrations of the samples were accurately determined without any indication of prediction bias or abnormality. The range of average percent errors was similar to the range of the RSDs of the peak intensities in the calibration curve.

The long-term stability of the sensor was tested by measuring a 10 ppb $As^{3+}$ sample over 3 days. On each day, 20 measurements were accomplished, resulting in a total of 60 continuous measurements. The peak intensities were steady up to the 50$^{th}$ measurement with RSD of 8.98% and started to decrease afterward. The decrease of signal was attributed to the partial detachment of nanodendrites from the frame, which was visually observable. Nonetheless, the sensor response was stable up to 50-cycle measurements, so acceptable to use as a field-applicable sensor.

For the selectivity test, an element calibration standard solution containing $Ag^+$, $Al^{3+}$, $As^{3+}$, $Ba^{2+}$, $Be^{2+}$, $Bi^{5+}$, $Ca^{2+}$, $Cd^{2+}$,

**Table 1** Results for the determination of $As^{3+}$ concentrations in three samples prepared in tap water using three independent CR-CNT/AuNDs

| | Predicted $As^{3+}$ concentration (ppb) | | | |
|---|---|---|---|---|
| | Sensor #1 | Sensor #2 | Sensor #3 | Average percent error (%) |
| 20.0 ppb As sample | 22.7 | 21.1 | 19.4 | 10.3 |
| 40.0 ppb As sample | 41.3 | 40.1 | 39.2 | 3.1 |
| 60.0 ppb As sample | 64.2 | 60.8 | 59.2 | 2.1 |

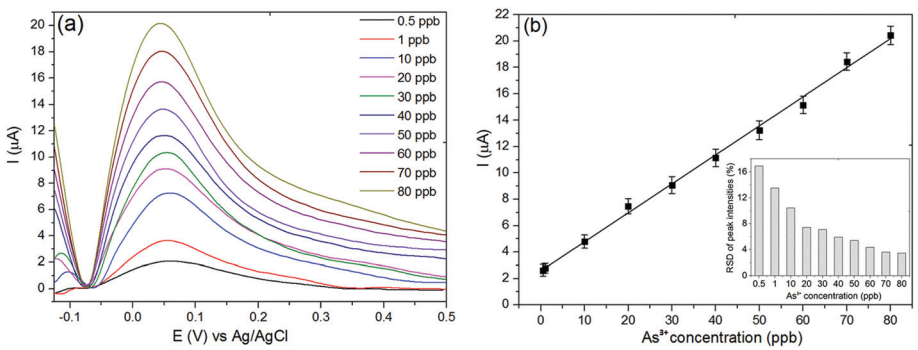


**Fig. 5** Stripping voltammograms acquired from ten $As^{3+}$ samples (concentration range: 0.5–80 ppb) using MPL-CNT/AuND (a) and a plot of the $As^{3+}$ concentration *vs.* the peak intensity (b). The inset shows the RSDs of the peak intensities in the voltammograms of each sample collected using three independent MPL-CNT/AuND sensors.

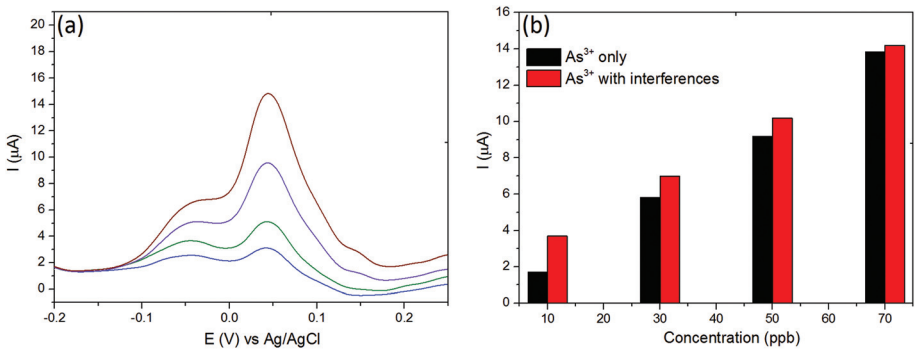


**Fig. 6** Stripping voltammograms acquired from four $As^{3+}$ samples contain all interfering ions with concentrations of 10, 30, 50 to 70 ppb (a) and the peak intensities acquired from the same As samples without (black) and with the interferences (red) (b).

$Co^{4+}$, $Cr^{6+}$, $Cs^{+}$, $Cu^{2+}$, $Fe^{3+}$, $Ga^{3+}$, $In^{3+}$, $K^{+}$, $Li^{+}$, $Mg^{2+}$, $Mn^{4+}$, $Na^{+}$, $Ni^{2+}$, $Pb^{4+}$, $Rb^{+}$, $Se^{6+}$, $Sr^{2+}$, $Tl^{3+}$, $U^{6+}$, $V^{5+}$ and $Zn^{2+}$ ions (a total 29 ions including $As^{3+}$) was used. Four samples, including all of the ions with concentrations of 10, 30, 50 to 70 ppb were prepared and their voltammograms were measured as shown in Fig. 6(a). In comparison with the voltammograms of pure $As^{3+}$ samples (Fig. 5(a)), the overall peak shape is moderately different and two small peaks at −0.05 and 0.15 V are observed; while the $As^{3+}$ peaks at 0.05 V remain clearly visible. The peak at −0.05 V is associated with $Cu^{2+}$, one of the main interferences in $As^{3+}$ detection as confirmed by measuring pure $Cu^{2+}$ samples using the same sensor. Fig. 6(b) shows the peak intensities acquired from 10, 30, 50 and 70 ppb $As^{3+}$ samples without (black) and with the interferences (red). As shown, the presence of interferences decreased the peak intensity and the relative decrease was more substantial when the concentration of $As^{3+}$ was lower, such as 53.9, 15.5, 9.8 and 2.4% for 10, 30, 50 and 70 ppb samples, respectively. The presence of $Cu^{2+}$ will interfere the measurement of $As^{3+}$, especially when its concentration is low such as below 50 ppb. Further, the selectivity of a sensor against $As^{5+}$, organic As (monomethyl arsenic acid) and $Hg^{2+}$ was separately tested as shown in the ESI.† In the cases of $As^{5+}$ and monomethyl arsenic acid, no significant electrochemical signals corresponding to them were observed. Meanwhile, $Hg^{2+}$ peaks increasing with the elevation of concentration were observed around 0.38 V; however, they did not overlap with the $As^{3+}$ peak located around 0.05 V. Therefore, the presence of $As^{5+}$, monomethyl arsenic acid and $Hg^{2+}$ will not hamper the measurement of $As^{3+}$.

Meanwhile, measurement of the sample at neutral pH is more facile without further pH adjustment to acidic conditions as performed in this study. For evaluation, the same samples were measured once again at neutral pH using the same sensor. The resulting response was also linear; while, the sensitivity (slope) decreased by 2.2-fold to 0.05 mA $ppb^{-1}$ and LOD increased by 4.25-fold to 1.7 ppb, compared with the performances shown in Fig. 5. Nonetheless, the proposed sensor still enables the sensitive detection of $As^{3+}$ in neutral samples.

## Conclusions

The performances of electrochemical measurements using MPL-CNT/AuND, such as the sensitivity and sensor-to-sensor reproducibility, were acceptable as a candidate for an inexpensive and easy-to-make electrochemical sensor. In addition, the current density was higher than that of a Pt-supported Au nanodendrite electrode. The use of CNTs during the electrodeposition made the sensor physically more durable. A small analytical device embedding MPL-CNT/AuND as a disposable electrochemical sensor is under development for the on-site measurement of diverse analytes. In parallel, MPLs of other grades containing different amounts of graphite/clay/wax will be evaluated as a sensor frame because the electrochemical performance and structural ruggedness of the resulting sensors would vary depending on MPL composition. The incorporation of composite metal nanostructures such as Au/Ag and Au/Ag/Pt is also underway to enhance the utility of MPL-based sensors.

## Acknowledgements

This research was supported by Basic Science Research Program through the National Research Foundation of Korea (NRF) funded by the Ministry of Science, ICT and Future Planning (NRF-2015R1A2A2A01006445) and Korea Ministry of Environment as The Converging Technology Program (grant number: ARQ201403075001).

## References

1 K. Kalcher, I. Švancara, R. Metelka, K. Vytřas and A. Walcarius, in *Encyclopaedia of Sensors*, ed. G. A. Crimes, E. C. Dickey and M. V. Pishko, American Scientific Publishers, Los Angeles, 2006, vol. 4, pp. 283–429.
2 H. E. Zittel and F. J. Miller, *Anal. Chem.*, 1965, **37**, 200–203.

 

3 K. Vytřas, I. Švancara and R. Metelka, *J. Serb. Chem. Soc.*, 2009, **74**, 1021–1033.
4 K. C. Honeychurch, *Insci. J.*, 2012, **2**, 1–51.
5 A. M. Bond, P. J. Mahon, J. Schiewe and V. Vicente-Beckett, *Anal. Chim. Acta*, 1997, **345**, 67–74.
6 D. King, J. Friend and J. Kariuki, *J. Chem. Educ.*, 2010, **87**, 507–509.
7 J. K. Kariuki, *J. Electrochem. Soc.*, 2012, **159**, H747–H751.
8 N. Chauhan, J. Narang and C. Pundir, *Am. J. Anal. Chem.*, 2010, **2**, 41–46.
9 D. Demetriades, A. Economou and A. Voulgaropoulos, *Anal. Chim. Acta*, 2004, **519**, 167–172.
10 K. Pokpas, S. Zbeda, N. Jahed, N. Mohamed, P. G. Baker and E. I. Iwuoha, *Int. J. Electrochem. Sci.*, 2014, **9**, 736–759.
11 M. Vestergaard, K. Kerman and E. Tamiya, *Anal. Chim. Acta*, 2005, **538**, 273–281.
12 Y. W. Hartati, S. Topkaya, I. P. Maksum and M. Ozsoz, *Adv. Anal. Chem.*, 2013, **3**, 20–27.
13 N. Dossi, R. Toniolo, F. Terzi, F. Impellizzieri and G. Bontempelli, *Electrochim. Acta*, 2014, **146**, 518–524.
14 J. Kariuki, E. Ervin and C. Olafson, *Sensors*, 2015, **15**, 18887–18900.
15 D. Kashyap, C. Kim, S. Y. Kim, Y. H. Kim, G. M. Kim, P. K. Dwivedi, A. Sharma and S. Goel, *Int. J. Hydrogen Energy*, 2015, **40**, 9515–9522.
16 U. Chandra, B. E. K. Swamy, O. Gilbert, S. Reddy and B. S. Sherigara, *Am. J. Anal. Chem.*, 2011, **2**, 262–269.
17 T. A. Bendikov and T. C. Harmon, *J. Chem. Educ.*, 2005, **82**, 439–441.
18 S. Teepoo, P. Chumsaeng, P. Nethan, W. Prueprang and P. Tumsae, *Int. J. Electrochem. Sci.*, 2012, **7**, 4645–4656.
19 C. Cheng, K. Chang, C. Chen and D. G. Pijanowska, *J. Chin. Chem. Soc.*, 2011, **58**, 739–748.
20 J. Narang, N. Malhotra, G. Singh and C. S. Pundir, *Biosens. Bioelectron.*, 2015, **66**, 332–337.
21 G. Congura, F. Sayar, A. Erdema and E. Piskin, *Colloids Surf., B*, 2013, **112**, 61–66.
22 T. N. Huan, T. Ganesh, K. S. Kim, S. Kim, S. Han and H. Chung, *Biosens. Bioelectron.*, 2011, **27**, 183–186.
23 P. K. Duy, P. T. H. Yen, S. Chun, V. T. T. Ha and H. Chung, *Sens. Actuators, B*, 2016, **225**, 377–383.
24 M. C. Sousa and J. W. Buchanan, *Comput. Graph. Forum*, 2000, **19**, 27–49.
25 A. Ressine, C. Vaz-Domínguez, V. Fernandez, A. De Lacey, T. Laurell, T. Ruzgas and S. Shleev, *Biosens. Bioelectron.*, 2010, **25**, 1001–1007.